An iron(II) complex shows bistable spin-state switching characteristic with $T_{1/2}$ centred at room temperature

Senthil Kumar Kuppusamy,[a*] Lea Spieker,[b] Benoît Heinrich,[c] Heiko Wende,[b] and Mario Ruben [a,d,e]

[a]Institute of Quantum Materials and Technologies (IQMT),
Karlsruhe Institute of Technology (KIT), Hermann-von-Helmholtz-Platz 1,
76344 Eggenstein-Leopoldshafen, Germany. E-mail : senthil.kuppusamy2@kit.edu

[b]University of Duisburg-Essen,
Faculty of Physics and Center for Nanointegration Duisburg-Essen (CENIDE),
Lotharstraße 1, 47057 Duisburg, Germany.

[c]Institut de Physique et Chimie des Matériaux de Strasbourg (IPCMS),
CNRS-Université de Strasbourg, 23, rue du Loess, BP 43,
67034 Strasbourg Cedex 2, France.

[d]Institute of Nanotechnology (INT),
Karlsruhe Institute of Technology (KIT),
Hermann-von-Helmholtz-Platz 1,
76344 Eggenstein-Leopoldshafen, Germany.

[e]Centre Européen de Sciences Quantiques (CESQ)
Institut de Science et d'Ingénierie, Supramoléculaires (ISIS),
8 allée Gaspard Monge, BP 70028,
67083 Strasbourg Cedex, France.

Abstract

An iron(II) complex (1·CH_3CN) composed of a tridentate all nitrogen coordinating ligand—ethyl 2,6-bis(1H-pyrazol-1-yl)isonicotinate (BPP-COOEt)—shows bistable spin-state switching characteristic with thermal hysteresis width ($\Delta T_{1/2}$) = 44 K and switching temperature ($T_{1/2}$) = 298 K in the first cycle. Crystal structures of the LS and HS forms of the complex reveal that spin-state switching induces a pronounced angular distortion, creating an energy barrier separating the LS and HS states. Traversing the barrier requires substantial molecular rearrangement in the presence of constraints imposed by the crystal lattice, rendering the spin-state switching of 1·CH_3CN hysteretic in the solid-state. The rare observation of bistable SCO with $T_{1/2}$ centred at room temperature (RT) renders the complex an ideal model system to study reversible spin-state tuning under ambient conditions.

Introduction

Molecular materials that show switching of a physical property—for example, magnetic[1–12] or electric[13–17]—accompanied with hysteresis are candidates desirable for applications. Several classes of magnetic-molecular systems such as organic radicals,[18,19] single-molecule magnets (SMMs), and spin-crossover complexes are all known to show bistable switching characteristic. However, to the best of our knowledge, SCO complexes are the only class of molecules that frequently show bistable switching near room-temperature (RT).[4,12] For realistic applications, SCO complexes showing a sizable thermal hysteresis width ($\Delta T_{1/2}$)—around 70 K—with switching centred around RT are required.[4] However, preparing an SCO complex that can undergo hysteretic switching around RT is not a trivial task because spin-state switching in the solid-state is controlled by a myriad of factors, which are system-dependent. Therefore, it is necessary to conduct a systematic search starting from a basic ligand skeleton featuring a moderate ligand field allowing spin-state switching of a coordinated metal ion, iron(II) in the context of this study. 2,6-bis(1H-pyrazol-1-yl)pyridine (BPP)-based ligands are a class of tridentate nitrogen-donor ligands that facilitate spin-state switching of the coordinated iron(II) centre, as first reported by Halcrow and co-workers in 2001.[20] The propensity to modify the BPP skeleton with functional groups at the pyridine and pyrazole rings allows systematic studying of spin-state switching of the resultant iron(II)-BPP complexes.[21] Recently, technologically relevant spin-state switching characteristics of iron(II) complexes a, b, c, and d (Figure 1) composed of a BPP-based ligand—ethyl 2,6-bis(1H-pyrazol-1-yl)isonicotinate (BPP-COOEt)—have been reported. The reports showed that SCO in the complexes is lattice solvent- and anion-dependent.[9,22,23] Such observations prompted us to further study the role of

lattice solvent in controlling SCO in iron(II) complexes composed of BPP-COOEt. Consequently, in this study, we report on the bistable spin-state characteristic of an iron(II) complex ($1\cdot CH_3CN$; Figure 1) based on BPP-COOEt ligand. Complex $1\cdot CH_3CN$ shows $\Delta T_{1/2}$ = 44 K with $T_{1/2}$ centred at RT (298 K) in the first cycle. However, the switching is not stable upon repeated cycling due to gradual lattice solvent release and self-grinding of the crystallites; therefore, the practical utility of the complex is unforeseeable. However, complex $1\cdot CH_3CN$ is a rare example of a mononuclear iron(II) complex that shows bistable SCO with $T_{1/2}$ centred at RT. Crucially, our attribution, as detailed in the following sections, that pronounced molecular distortion contributes to the opening of thermal hysteresis loop could enable future designs of iron(II)-based SCO complexes with technologically relevant spin-state switching characteristics.

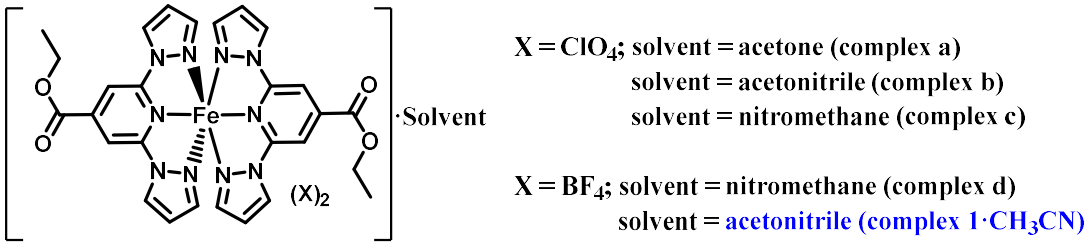

Figure 1. Ethyl 2,6-bis(1H-pyrazol-1-yl)isonicotinate (BPP-COOEt)-based iron(II) complexes—a, b, c, and d—studied previously[9,22,23] and in this study ($1\cdot CH_3CN$).

Results

Preparation of complex $1\cdot CH_3CN$

Ligand BPP-COOEt was synthesized following a previously reported procedure.[24] Treatment of $Fe(BF_4)_2\cdot 6H_2O$ as a solid with the acetonitrile solution of the ligand yielded a wine-red solution, indicating complex formation (Scheme 1). Slow diffusion of diethyl ether into the acetonitrile solution of the complex at 4 °C over a period of 2-3 weeks yielded wine-red crystals suitable for single-crystal X-ray diffraction (SC-XRD) studies. In one such crystallization attempt, a few yellow crystals suitable for the SC-XRD studies were also obtained along with the wine-red crystals.

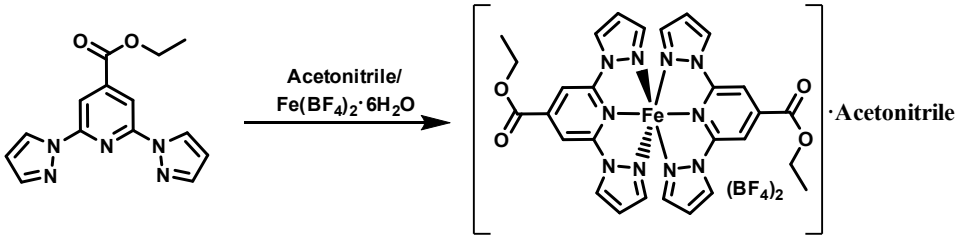

BPP-COOEt **Complex 1·CH_3CN**

Scheme 1. Preparation of complex 1·CH_3CN.

After harvesting from the mother liquor, the wine-red crystals were washed with ether and dried under vacuum for 4 h. Elemental analysis of the dried crystals revealed that lattice acetonitrile solvent is retained after the drying process.

X-ray crystal structures of the low spin (LS) and high spin (HS) forms of complex 1·CH_3CN

Structure determination of wine-red (173 K) and yellow (293 K) crystals (Figure 2 and Table 1) revealed that the complexes are in the LS and HS states, respectively, as inferred from the Fe-N bond lengths and angular parameters collected in Table 2. The complexes crystallized with one molecule of acetonitrile in the lattice.

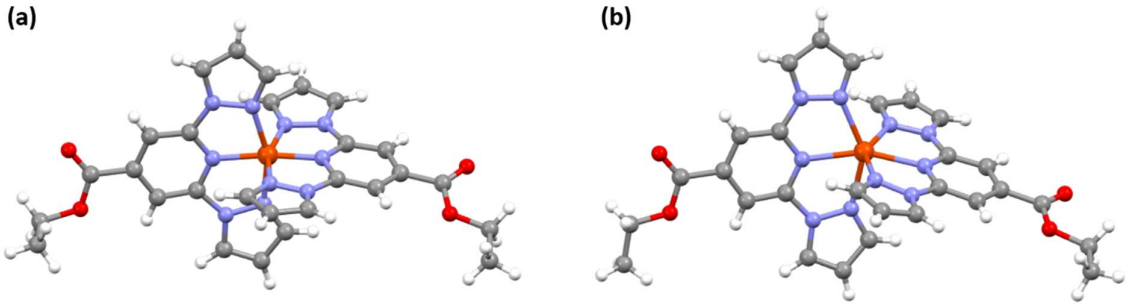

Figure 2. Single-crystal X-ray structures of the (a) LS and (b) HS forms of 1·CH_3CN determined at 173 K and 293 K, respectively. The lattice acetonitrile molecules and BF_4 anions are not shown for clarity. The spin-state switching is accompanied with conformational switching of one of the ethyl substituents and pronounced angular distortion.

Table 1. Crystallographic data of LS[a] and HS[b] forms of 1·CH_3CN.

	1·CH_3CN (LS, 173 K)	1·CH_3CN (HS, 293 K)
Formula	$C_{30}H_{29}B_2F_8FeN_{11}O_4$	$C_{30}H_{29}B_2F_8FeN_{11}O_4$
FW/g.mol^{-1}	837.11	837.11
T/K	173	293
Crystal System	Monoclinic	Monoclinic

Space group	*P21/c*	*P21/n*
a/Å	10.6227(2)	9.694(3)
b/Å	23.8289(5)	25.264(6)
c/Å	16.4258(3)	15.183(2)
α/°	90 (1)	90
β/°	119.508(1)	96.941(11)
γ/°	90	90
V/Å^3	3618.50 (13)	3691.3(12)
Z	4	4
ρ/g.cm^{-3}	1.537	1.506
μ/mm^{-1}	4.190	0.501
R1	0.0573	0.0902
wR2	0.1496	0.2693

[a] ccdc 1560719, [b] ccdc 2194264

Table 2. Selected bond lengths (Å), angles, and angular parameters (°) of the LS and HS forms of 1·CH_3CN.

Parameter	1·CH_3CN (LS)	1·CH_3CN (HS)
T/K	173	293
Fe_1-N_1(pyrazolyl)	1.962(3)	2.148
Fe_1-N_3(pyridyl)	1.899(3)	2.137
Fe_1-N_5 (pyrazolyl)	1.976(3)	2.178
Fe_1-N_6 (pyrazolyl)	1.975(3)	2.185
Fe_1-N_8 (pyridyl)	1.887(3)	2.144
Fe_1-N_{10} (pyrazolyl)	1.953(3)	2.160
rFe-N	1.942	2.158(6)
N_3-Fe_1-N_8 (ϕ)	172.87(12)	159.45
N_6-Fe_1-N_{10} (ψ)	160.53(12)	146.04
N_1-Fe_1-N_5 (ψ)	160.43(12)	145.69
θ	86.70	80.08

On a comparative scale, the HS-form features a distorted coordination geometry relative to its LS counterpart. Such distortion in the crystal lattice is known to induce spin-state switching with a wide hysteresis loop, as reported for the BPP-based[9,23] and related systems.[4]

Spin-state switching characteristics of 1·CH$_3$CN

Magnetic susceptibility measurements of gently ground wine-red crystals were performed under 0.1 T applied magnetic field. A scan rate of 2 K min^{-1} was employed, and the data were collected in the settle mode.

The complex exhibited abrupt SCO with 44 K and 52 K hysteresis loops for the first ($T_{1/2\uparrow}$ = 320 K and $T_{1/2\downarrow}$ = 276 K) and second ($T_{1/2\uparrow}$ = 320 K and $T_{1/2\downarrow}$ = 268 K) heating-cooling cycles, respectively, as depicted in Figure 3. The obtained χT products of 3.18 cm^3 K mol^{-1} and 0.18 cm^{3}Kmol^{-1} at 335 K and 200 K, respectively, for the first cycle, reveal the presence of pure HS and predominantly LS species at those temperatures—a genuine temperature-induced spin-state switching is inferred. Further cycling resulted in a steady decrease of the χT product (Figure 3 and Table 3) indicating the increase of the trapped LS state and unstable nature of the spin-state switching characteristic of the complex to repeated thermal scanning.

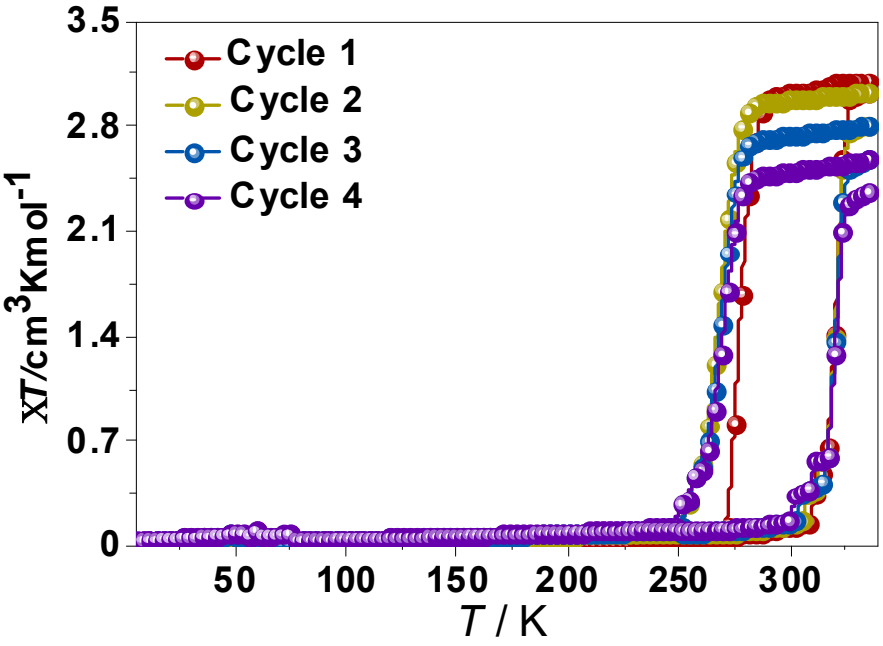

Figure 3. Spin-state switching characteristic of 1·CH$_3$CN. χT versus T plots of the complex showing bistable—abrupt and hysteretic—spin-state switching characteristic with $\Delta T_{1/2}$ = 44 K and $T_{1/2}$ = 298 K (cycle 1).

To check for the reproducible nature of the spin-state switching, a fresh crop of wine-red crystals of the complex was grown, and the spin-state switching characteristic of the sample was studied by repeatedly subjecting it to thermal scanning from 335 K-to-5 K, and vice versa (Figure 4). The $T_{1/2}$ and $\Delta T_{1/2}$ values obtained from the first cycle are comparable with the ones obtained from the measurements shown in Figure 3. Upon repeated scanning, a steady decrease of χT values was observed until the 11th scan. Further scanning resulted in a stabilized χT versus T plots with the sample trapped in a mixed spin phase predominantly composed of LS complexes. The incremental spin-state evolution in response to repeated cycling is attributed to self-grinding effect[25] and the concomitant gradual lattice solvent loss (*vide infra*). The cycling is also accompanied by a steady rise of χT value in the 5 K-to-275 K region, as recently observed for an iron(II)-BPP system by Halcrow and co-workers.[26] A fraction of the complex molecules in the mixed phase, obtained after the 11th cycle, undergoes gradual SCO, as depicted in Figure 4.

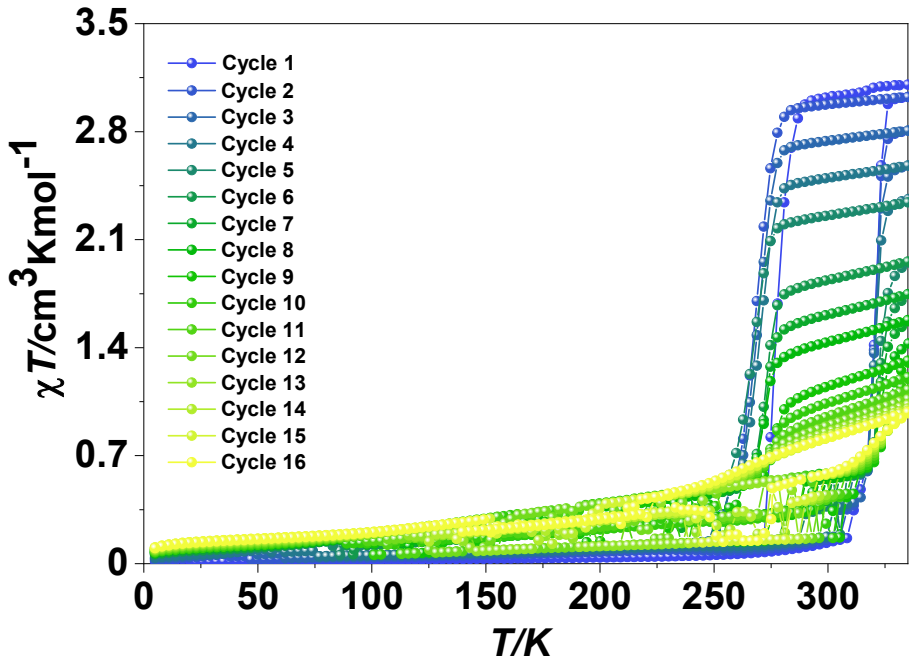

Figure 4. Spin-state switching characteristics of 1·CH$_3$CN upon repeated cycling. χT versus T plots of wine-red crystals of 1·CH$_3$CN. A second set of freshly prepared crystals were used for the measurements.

Table 3. Parameters associated with the SCO of 1·CH_3CN.

	SQUID			DSC	
	χT (HS)/cm^3Kmol^{-1}	$T_{1/2}$/K	ΔT/K	$T_{1/2}$/K	ΔT/K
Cycle 1	3.18	298	44	298	44
Cycle 2	3.02	294	52	294	56
Cycle 3	2.79	294	51	293	60
Cycle 4	2.56	295	50	292	66

To further confirm the occurrence of temperature-induced spin-state switching in 1·CH_3CN, differential scanning calorimetric (DSC) studies were performed, as shown in Figure 5a. The $T_{1/2}$ and $\Delta T_{1/2}$ values obtained from the DSC studies (Table 3) are in good agreement with the values obtained from the magnetic measurements shown in Figure 3, confirming the bistable spin-state switching characteristic of 1·CH_3CN.

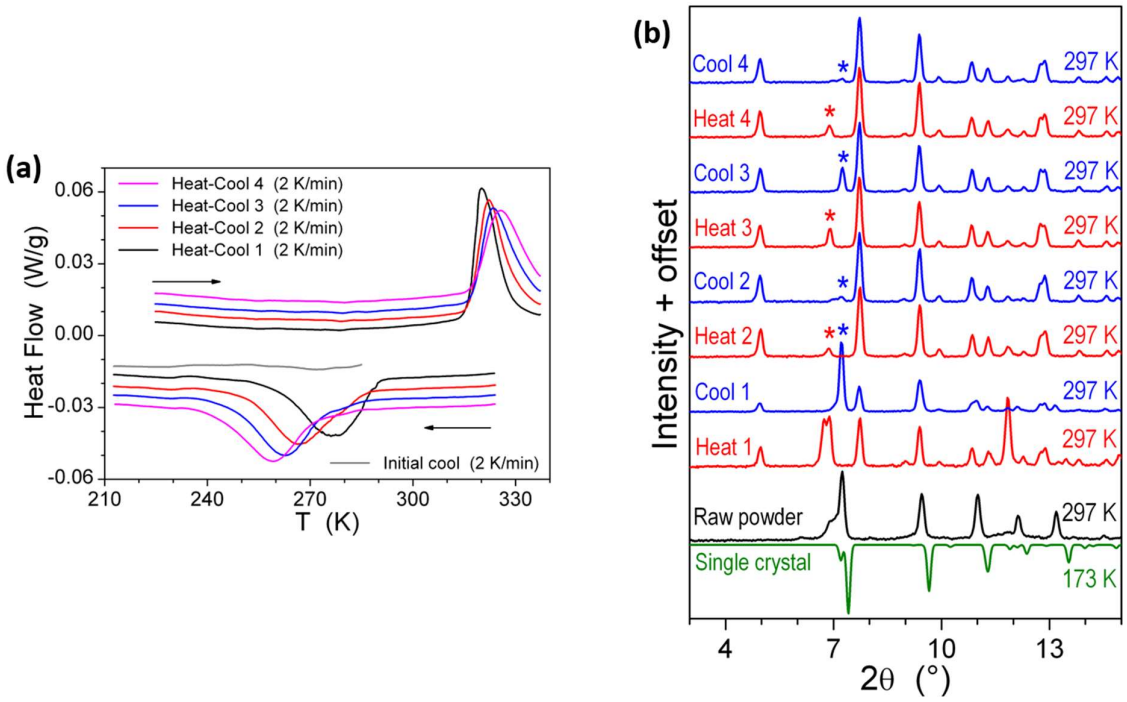

Figure 5. Differential scanning calorimetric (DSC) and small- and wide-angle X-ray scattering (SWAXS) studies of complex 1·CH_3CN. (a) DSC profiles showing temperature-induced spin-state switching in the 210 K-to-330 K temperature range. (b) SWAXS patterns of 1·CH_3CN showing continuously evolving crystalline phases in response to repeated heat-cool cycling. The patterns were collected at 297 K after heating and cooling the sample ex-situ at 330 K and 77 K, respectively.

Our attempts to reversibly cycle single-crystals of $1{\cdot}CH_3CN$ from the LS state to the HS state inside the diffractometer were not successful due to the explosion of the crystals when heated in the vicinity of spin-transition temperature. Similar attempts with the HS crystals met with the same fate while cooling them. Such unsuccessful attempts with the single-crystals led us to study complex $1{\cdot}CH_3CN$ with the help of small- and wide-angle X-ray scattering (SWAXS) studies to get a glimpse of lattice variations during the spin-state switching process. As shown in figure 5b, the SWAXS pattern obtained from a ground sample of $1{\cdot}CH_3CN$ is comparable with the calculated pattern obtained from the single-crystal data. The differences between the SWAXS and calculated patterns obtained at 293 K and 173 K, respectively, are attributed to temperature- and grinding-induced variation of lattice parameters. Such attribution is based on our recent observation of grinding-mediated loss of crystallinity of complex c (Figure 1).[23] Repeated heat-cool cycles of ground $1{\cdot}CH_3CN$ caused an irreversible drift superposed with SCO modulation of diffraction profiles, serving as an in-situ proof of the thermal-cycling-mediated evolution of the high- and low-temperature crystalline phases. A comparison between the results obtained from the magnetic and SWAXS studies led us to the following conclusion: the two initial structures—heat 1 (HS) and cool 1 (LS) in Figure 5b—have different lattice features showing that the SCO is coupled with a lattice parameter variation, as also evidenced from the SC-XRD studies (Figure 2 and Table 1-2). In the subsequent cycles, the spin-state switching characteristics are incrementally modified by the gradual removal of solvent molecules, leading to the formation of two stable solvent-free phases complying both with LS-states.

To shed light on the fate of lattice acetonitrile in $1{\cdot}CH_3CN$ during the repeated heat-cool cycling, thermogravimetric analyses (TGA) of various forms of the complex were performed. The crystalline $1{\cdot}CH_3CN$ underwent a 5% weight loss around 400 K, corresponding to the loss of one molecule of acetonitrile from the lattice (Figure 6a). On the contrary, no such weight loss is observed for a sample dried at 423 K (Figure 6a), revealing the complete removal of acetonitrile molecule from the lattice. TGA analysis of the sample obtained after SWAXS studies also showed a lack of pronounced weight loss (Figure 6b). Actually, the TGA profiles of the deliberately desolvated sample at 423 K and the sample obtained after the repeated SWAXS measurements are comparable. Based on the above observations, we conclude that repeated spin-state switching of $1{\cdot}CH_3CN$ is accompanied with a gradual loss of lattice acetonitrile molecules, forming $1{\cdot}xCH_3CN$ ($x < 1$) lattice with varying solvent content before the formation of solvent-free 1. Note that the solvent removal process during the SWAXS

measurements is accelerated due to the ex-situ heating and cooling of the sample, which is in contrast to the magnetic measurements performed inside a SQUID cavity. The almost complete loss of lattice solvent after four external heat-cool cycles during the SWAXS studies is justified based on the above argument.

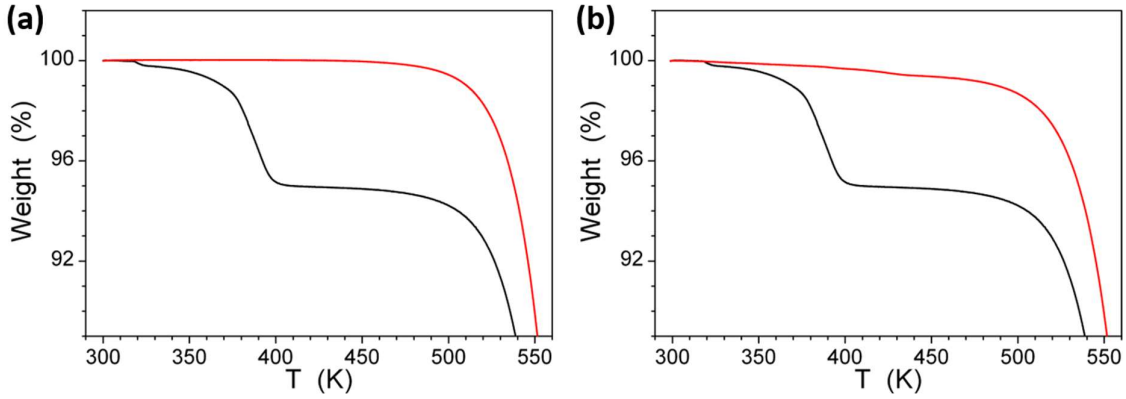

Figure 6. Thermogravimetric analyses (TGA) of 1·CH$_3$CN. (a) TGA of 1·CH$_3$CN (black curve) and its solvent-free version (red curve). (b) TGA of 1·CH$_3$CN ((black curve) and the sample obtained after four cycles of SWAXS measurements ((red curve) shown in Figure 5b.

Discussion

The first synthesis of BPP-COOEt ligand used to prepare 1·CH$_3$CN reported in this study was reported almost 20 years before.[24] However, the utility of the ligand to prepare iron(II)-based mononuclear complexes was not reported until 2018.[22] The first reported iron(II) complex (a, Figure 1) of the ligand, showed an irreversible LS-to-HS switching with the switching temperature centred around 330 K. Once heated above 350 K, complex a lost the lattice acetone solvent and the solvent-free version was trapped in the HS-state in the subsequent cooling. Our attempts to study similar complexes as acetonitrile (complex b; Figure 1) and nitromethane (complexes c and d; Figure 1) solvates led to the observation of hysteretic spin-state switching.[9,23] Remarkably, complex c showed stable hysteretic spin-state switching characteristics with $T_{1/2} = 288$ K; $\Delta T_{1/2} = 62$ K.[23] In a different scenario, Sato and co-workers used BPP-COOEt to prepare a mononuclear cobalt(II) complex, which underwent switching of orbital angular momentum due to switching of coordination number from seven-to-six, and vice versa,[27] demonstrating an altogether different switching mechanism contrast to the spin-multiplicity-based switching demonstrated in this study. The above discussion indicates that coordination complexes based on a simple ligand system such as BPP-COOEt can feature exotic magnetic properties.

In a recent study, we observed pronounced molecular distortion upon spin-state switching of complexes c and d (Figure 1).[23] Such distortion coupled with conformational variation of the Et group stabilizes the complexes either in a LS- or HS-state; creating an energy barrier, thereby thermal hysteresis loops are observed upon spin-state switching. Recently, Real and co-workers reported a mononuclear iron(II) complex with a wide 105 K thermal hysteresis loop and $\Delta T_{1/2}$ =~308 K. They elucidated that molecular distortion and conformational switching cause hysteretic spin-state switching associated with the complex.[4] The angular parameters collected in Table 2 reveal that the HS-form of complex 1·CH_3CN features a distorted molecular geometry relative to its LS counterpart showing close to the ideal octahedral geometry. The obtained variations in ϕ and θ—$\Delta\phi$ = 13.42° and $\Delta\theta$ = 6.62°—indicate that the complex needs to traverse a significant energy barrier to switch from one spin-state to another; that is, HS-to-LS and vice versa. Moreover, conformation of one of the ethyl groups of 1·CH_3CN varies upon spin-state switching (Figure 2). Based on the SC-XRD data and previous studies discussed above, we attribute the origin of the 44 K thermal hysteresis width observed for 1·CH_3CN to the pronounced molecular distortion and ethyl group conformational variation. Note that the HS-form of the complex is obtained after a chance crystallization, and we were unable to generate the HS-form in-situ, as afore discussed.

Overall, complex 1·CH_3CN reported in this study is one of the rare mononuclear iron(II) spin-crossover complexes showing hysteretic spin-state switching with $T_{1/2}$ centred at RT. However, the SCO is lattice-solvent-dependent, and the solvent loss accompanying the spin state switching process combines with significant variations of the crystalline structures, as inferred from the SWAXS studies. Such aspects render the SCO unstable to thermal cycling, impeding the practical utility of the complex as a molecular switch or memory. On the positive side, the attribution that pronounced angular distortion and conformational variation of ethyl group contribute to the opening of thermal hysteresis in 1·CH_3CN adds to the extensive knowledge collected on SCO systems over almost a century. As a perspective, the pronounced distortion associated with the HS-state of 1·CH_3CN and lattice constraints hindering the HS-to-LS switching could confer the HS-state of the complex with a long lifetime, enabling reversible addressing of the spin-states at RT. Finally, the grand old phenomenon of SCO continues to evolve keeping abreast with the contemporary developments in molecular magnetism and related topics.[5,28–39] We are happy that the topic has chosen us to express interesting facets, as discussed in this script.

Experimental

Materials

Anhydrous solvents and $Fe(BF_4)_2 \cdot 6H_2O$ were purchased from commercial sources and used as received. Glassware were dried in a vacuum oven at 150 °C prior to the experiments. All the complexation reactions were performed under argon (Ar) atmosphere.

Synthesis of BPP-COOEt ligand (L) and complex 1

Ligand L was synthesized according to the literature procedure.[24]

Ligand (L) (0.058g, 0.2 mmol) was solubilized in 10 ml of ACN. To this $[Fe(BF_4)_2] \cdot 6H_2O$ (0.1 mmol) was added and the mixture was stirred at RT for 2 h under Ar atmosphere. The reaction mixture was filtered and portioned into test tubes followed by isothermal diffusion of Et_2O at 4 °C over a period of 2-3 weeks yielded good quality crystals suitable for X-ray analysis. Formation of a nearly colorless solution is considered as an end point of the crystallization process.

Yield of complex 1: 46 mg (60%).

Elemental analysis: calc for $C_{28}H_{26}B_2F_8FeN_{10}O_4 \cdot CH_3CN$: C, 43.05; H, 3.49; N; 18.41. Found: C, 42.7, H, 3.5, N, 18.28.

Physical measurements

Magnetic measurements of the complex were performed on a MPMS-3 SQUID-VSM magnetometer (Quantum Design). The temperature-dependent magnetization was recorded at an applied DC field of 0.1 T. A temperature sweeping rate of 2 K min^{-1} was employed, unless otherwise noted. Gelatine capsules were used as sample holders in the 5 K to 335 K temperature range.

Small- and wide-angle X-ray scattering (SWAXS) patterns of the complex were obtained with a linear monochromatic Cu $K_{\alpha 1}$ beam (λ = 1.5405 Å). The beam was obtained using a sealed-tube generator equipped with a bent quartz monochromator. The samples were filled in sealed cells of adjustable path. The sample temperature was controlled within ±0.1 °C, and exposure times were of 24 h. The patterns were recorded on image plates scanned by Amersham Typhoon IP with 25 µm resolution (periodicities up to 120 Å). I(2θ) profiles were obtained from images, by using a home-developed software.

Thermogravimetric analyses were performed with a TA Instruments Q50 instrument operated at a scanning rate of 5 K/min.

Elemental analyses of the complex was performed using Elementar vario MICRO cube elemental analyser.

Acknowledgements

Grant Agency Innovation FRC is acknowledged for the financial support for the project Self-assembly of spin-crossover (SCO) complexes on graphene. M.R. thanks the DFG priority program 1928 "COORNETS" for generous support. L.S and H.W. acknowledge the funding by the Deutsche Forschungsgemeinschaft (DFG, German Research Foundation)–Project-ID 278162697 – CRC 1242, Project A05.

References

(1) Sato, O. Dynamic Molecular Crystals with Switchable Physical Properties. *Nat. Chem.* **2016**, *8* (7), 644–656. https://doi.org/10.1038/nchem.2547.

(2) Sessoli, R.; Gatteschi, D.; Caneschi, A.; Novak, M. A. Magnetic Bistability in a Metal-Ion Cluster. *Nature* **1993**, *365* (6442), 141–143. https://doi.org/10.1038/365141a0.

(3) Ishikawa, N.; Sugita, M.; Ishikawa, T.; Koshihara, S.; Kaizu, Y. Lanthanide Double-Decker Complexes Functioning as Magnets at the Single-Molecular Level. *J. Am. Chem. Soc.* **2003**, *125* (29), 8694–8695. https://doi.org/10.1021/ja029629n.

(4) Seredyuk, M.; Znovjyak, K.; Valverde-Muñoz, F. J.; da Silva, I.; Muñoz, M. C.; Moroz, Y. S.; Real, J. A. 105 K Wide Room Temperature Spin Transition Memory Due to a Supramolecular Latch Mechanism. *J. Am. Chem. Soc.* **2022**, jacs.2c05417. https://doi.org/10.1021/jacs.2c05417.

(5) Wu, S.-G.; Wang, L.-F.; Ruan, Z.-Y.; Du, S.-N.; Gómez-Coca, S.; Ni, Z.-P.; Ruiz, E.; Chen, X.-M.; Tong, M.-L. Redox-Programmable Spin-Crossover Behaviors in a Cationic Framework. *J. Am. Chem. Soc.* **2022**, jacs.2c06313. https://doi.org/10.1021/jacs.2c06313.

(6) Gallé, G.; Deldicque, D.; Degert, J.; Forestier, Th.; Létard, J.-F.; Freysz, E. Room Temperature Study of the Optical Switching of a Spin Crossover Compound inside Its Thermal Hysteresis Loop. *Appl. Phys. Lett.* **2010**, *96* (4), 041907. https://doi.org/10.1063/1.3294312.

(7) Weber, B.; Bauer, W.; Obel, J. An Iron(II) Spin-Crossover Complex with a 70 K Wide Thermal Hysteresis Loop. *Angew. Chem. Int. Ed.* **2008**, *47* (52), 10098–10101. https://doi.org/10.1002/anie.200802806.

(8) Brooker, S. Spin Crossover with Thermal Hysteresis: Practicalities and Lessons Learnt. *Chem. Soc. Rev.* **2015**, *44* (10), 2880–2892. https://doi.org/10.1039/C4CS00376D.

(9) Senthil Kumar, K.; Heinrich, B.; Vela, S.; Moreno-Pineda, E.; Bailly, C.; Ruben, M. Bi-Stable Spin-Crossover Characteristics of a Highly Distorted [Fe(1-BPP-$COOC_2H_5$)$_2$](ClO_4)$_2$·CH_3CN Complex. *Dalton Trans.* **2019**, *48* (12), 3825–3830. https://doi.org/10.1039/C8DT04928A.

(10) Kahn, O.; Kröber, J.; Jay, C. Spin Transition Molecular Materials for Displays and Data Recording. *Adv. Mater.* **1992**, *4* (11), 718–728. https://doi.org/10.1002/adma.19920041103.

(11) Halcrow, M. A. Spin-Crossover Compounds with Wide Thermal Hysteresis. *Chem. Lett.* **2014**, *43* (8), 1178–1188. https://doi.org/10.1246/cl.140464.

(12) Schäfer, B.; Rajnák, C.; Šalitroš, I.; Fuhr, O.; Klar, D.; Schmitz-Antoniak, C.; Weschke, E.; Wende, H.; Ruben, M. Room Temperature Switching of a Neutral Molecular Iron(Ii) Complex. *Chem. Commun.* **2013**, *49* (93), 10986. https://doi.org/10.1039/c3cc46624h.
(13) Horiuchi, S.; Tokura, Y. Organic Ferroelectrics. *Nat. Mater.* **2008**, *7* (5), 357–366. https://doi.org/10.1038/nmat2137.
(14) Tayi, A. S.; Shveyd, A. K.; Sue, A. C.-H.; Szarko, J. M.; Rolczynski, B. S.; Cao, D.; Kennedy, T. J.; Sarjeant, A. A.; Stern, C. L.; Paxton, W. F.; Wu, W.; Dey, S. K.; Fahrenbach, A. C.; Guest, J. R.; Mohseni, H.; Chen, L. X.; Wang, K. L.; Stoddart, J. F.; Stupp, S. I. Room-Temperature Ferroelectricity in Supramolecular Networks of Charge-Transfer Complexes. *Nature* **2012**, *488* (7412), 485–489. https://doi.org/10.1038/nature11395.
(15) Liu, H.; Ye, Y.; Zhang, X.; Yang, T.; Wen, W.; Jiang, S. Ferroelectricity in Organic Materials: From Materials Characteristics to *de Novo* Design. *J. Mater. Chem. C* **2022**, 10.1039.D2TC01330D. https://doi.org/10.1039/D2TC01330D.
(16) Mohapatra, S.; Cherifi-Hertel, S.; Kuppusamy, S. K.; Schmerber, G.; Arabski, J.; Gobaut, B.; Weber, W.; Bowen, M.; Da Costa, V.; Boukari, S. Organic Ferroelectric Croconic Acid: A Concise Survey from Bulk Single Crystals to Thin Films. *J. Mater. Chem. C* **2022**, *10* (21), 8142–8167. https://doi.org/10.1039/D1TC05310H.
(17) Horiuchi, S.; Tokunaga, Y.; Giovannetti, G.; Picozzi, S.; Itoh, H.; Shimano, R.; Kumai, R.; Tokura, Y. Above-Room-Temperature Ferroelectricity in a Single-Component Molecular Crystal. *Nature* **2010**, *463* (7282), 789–792. https://doi.org/10.1038/nature08731.
(18) Fujita, W.; Awaga, and K. Room-Temperature Magnetic Bistability in Organic Radical Crystals. *Science* **1999**, *286* (5438), 261–262. https://doi.org/10.1126/science.286.5438.261.
(19) Paul, A.; Gupta, A.; Konar, S. Magnetic Transition in Organic Radicals: The Crystal Engineering Aspects. *Cryst. Growth Des.* **2021**, *21* (10), 5473–5489. https://doi.org/10.1021/acs.cgd.1c00731.
(20) Holland, J. M.; Kilner, C. A.; Thornton-Pett, M.; Halcrow, M. A.; McAllister, J. A.; Lu, Z. An Unusual Abrupt Thermal Spin-State Transition in $[FeL_2][BF_4]_2$ [L = 2,6-Di(Pyrazol-1-Yl)Pyridine]. *Chem. Commun.* **2001**, No. 6, 577–578. https://doi.org/10.1039/b100995h.
(21) Halcrow, M. A. Iron(II) Complexes of 2,6-Di(Pyrazol-1-Yl)Pyridines—A Versatile System for Spin-Crossover Research. *Coord. Chem. Rev.* **2009**, *253* (21–22), 2493–2514. https://doi.org/10.1016/j.ccr.2009.07.009.
(22) García-López, V.; Palacios-Corella, M.; Abhervé, A.; Pellicer-Carreño, I.; Desplanches, C.; Clemente-León, M.; Coronado, E. Spin-Crossover Compounds Based on Iron(II) Complexes of 2,6-Bis(Pyrazol-1-Yl)Pyridine (Bpp) Functionalized with Carboxylic Acid and Ethyl Carboxylic Acid. *Dalton Trans.* **2018**, *47* (47), 16958–16968. https://doi.org/10.1039/C8DT03511C.
(23) Suryadevara, N.; Mizuno, A.; Spieker, L.; Salamon, S.; Sleziona, S.; Maas, A.; Pollmann, E.; Heinrich, B.; Schleberger, M.; Wende, H.; Kuppusamy, S. K.; Ruben, M. Structural Insights into Hysteretic Spin-Crossover in a Set of Iron(II)-2,6-bis(1 *H* -Pyrazol-1-yl)Pyridine) Complexes. *Chem. – Eur. J.* **2022**, *28* (6). https://doi.org/10.1002/chem.202103853.
(24) Vermonden, T.; Branowska, D.; Marcelis, A. T. M.; Sudhölter, E. J. R. Synthesis of 4-Functionalized Terdendate Pyridine-Based Ligands. *Tetrahedron* **2003**, *59* (27), 5039–5045. https://doi.org/10.1016/S0040-4020(03)00753-1.
(25) Miyazaki, Y.; Nakamoto, T.; Ikeuchi, S.; Saito, K.; Inaba, A.; Sorai, M.; Tojo, T.; Atake, T.; Matouzenko, G. S.; Zein, S.; Borshch, S. A. Spin Crossover Phenomenon

Accompanying Order−Disorder Phase Transition in the Ligand of [Fe ^{II} (DAPP)(Abpt)]$(ClO_4)_2$ Compound (DAPP = Bis(3-Aminopropyl)(2-Pyridylmethyl)Amine, Abpt = 4-Amino-3,5-Bis(Pyridin-2-Yl)-1,2,4-Triazole) and Its Successive Self-Grinding Effect. *J. Phys. Chem. B* **2007**, *111* (43), 12508–12517. https://doi.org/10.1021/jp0730287.

(26) Kulmaczewski, R.; Kershaw Cook, L. J.; Pask, C. M.; Cespedes, O.; Halcrow, M. A. Iron(II) Complexes of 4-(Alkyldisulfanyl)-2,6-Di(Pyrazolyl)Pyridine Derivatives. Correlation of Spin-Crossover Cooperativity with Molecular Structure Following Single-Crystal-to-Single-Crystal Desolvation. *Cryst. Growth Des.* **2022**, *22* (3), 1960–1971. https://doi.org/10.1021/acs.cgd.2c00005.

(27) Su, S.-Q.; Wu, S.-Q.; Baker, M. L.; Bencok, P.; Azuma, N.; Miyazaki, Y.; Nakano, M.; Kang, S.; Shiota, Y.; Yoshizawa, K.; Kanegawa, S.; Sato, O. Quenching and Restoration of Orbital Angular Momentum through a Dynamic Bond in a Cobalt(II) Complex. *J. Am. Chem. Soc.* **2020**, *142* (26), 11434–11441. https://doi.org/10.1021/jacs.0c02257.

(28) Vallone, S. P.; Tantillo, A. N.; dos Santos, A. M.; Molaison, J. J.; Kulmaczewski, R.; Chapoy, A.; Ahmadi, P.; Halcrow, M. A.; Sandeman, K. G. Giant Barocaloric Effect at the Spin Crossover Transition of a Molecular Crystal. *Adv. Mater.* **2019**, *31* (23), 1807334. https://doi.org/10.1002/adma.201807334.

(29) Zhao, L.; Meng, Y.-S.; Liu, Q.; Sato, O.; Shi, Q.; Oshio, H.; Liu, T. Switching the Magnetic Hysteresis of an [Fe^{II}–NC–W^{V}]-Based Coordination Polymer by Photoinduced Reversible Spin Crossover. *Nat. Chem.* **2021**, *13* (7), 698–704. https://doi.org/10.1038/s41557-021-00695-1.

(30) Gavara-Edo, M.; Córdoba, R.; Valverde-Muñoz, F. J.; Herrero-Martín, J.; Real, J. A.; Coronado, E. Electrical Sensing of the Thermal and Light-Induced Spin Transition in Robust Contactless Spin-Crossover/Graphene Hybrid Devices. *Adv. Mater.* **2022**, 2202551. https://doi.org/10.1002/adma.202202551.

(31) Kumar, B.; Paul, A.; Mondal, D. J.; Paliwal, P.; Konar, S. Spin-State Modulation in Fe ^{II} -Based Hofmann-Type Coordination Polymers: From Molecules to Materials. *Chem. Rec.* **2022**. https://doi.org/10.1002/tcr.202200135.

(32) Oppermann, M.; Zinna, F.; Lacour, J.; Chergui, M. Chiral Control of Spin-Crossover Dynamics in Fe(II) Complexes. *Nat. Chem.* **2022**, *14* (7), 739–745. https://doi.org/10.1038/s41557-022-00933-0.

(33) Jiang, Y.; Liu, L. C.; Müller-Werkmeister, H. M.; Lu, C.; Zhang, D.; Field, R. L.; Sarracini, A.; Moriena, G.; Collet, E.; Miller, R. J. D. Structural Dynamics upon Photoexcitation in a Spin Crossover Crystal Probed with Femtosecond Electron Diffraction. *Angew. Chem. Int. Ed.* **2017**, *56* (25), 7130–7134. https://doi.org/10.1002/anie.201702497.

(34) Su, S.-Q.; Wu, S.-Q.; Huang, Y.-B.; Xu, W.-H.; Gao, K.-G.; Okazawa, A.; Okajima, H.; Sakamoto, A.; Kanegawa, S.; Sato, O. Photoinduced Persistent Polarization Change in a Spin Transition Crystal. *Angew. Chem. Int. Ed.* **2022**, anie.202208771. https://doi.org/10.1002/anie.202208771.

(35) Xue, J.-P.; Hu, Y.; Zhao, B.; Liu, Z.-K.; Xie, J.; Yao, Z.-S.; Tao, J. A Spin-Crossover Framework Endowed with Pore-Adjustable Behavior by Slow Structural Dynamics. *Nat. Commun.* **2022**, *13* (1), 3510. https://doi.org/10.1038/s41467-022-31274-8.

(36) Akiyoshi, R.; Hayami, S. Ferroelectric Coordination Metal Complexes Based on Structural and Electron Dynamics. *Chem. Commun.* **2022**, *58* (60), 8309–8321. https://doi.org/10.1039/D2CC02484E.

(37) Johannsen, S.; Ossinger, S.; Grunwald, J.; Herman, A.; Wende, H.; Tuczek, F.; Gruber, M.; Berndt, R. Spin Crossover in a Cobalt Complex on Ag(111). *Angew. Chem. Int. Ed.* **2022**, *61* (12). https://doi.org/10.1002/anie.202115892.

(38) Johannsen, S.; Schüddekopf, S.; Ossinger, S.; Grunwald, J.; Tuczek, F.; Gruber, M.; Berndt, R. Three-State Switching of an Fe Spin Crossover Complex. *J. Phys. Chem. C* **2022**, *126* (16), 7238–7244. https://doi.org/10.1021/acs.jpcc.2c00473.
(39) Li, D.; Tong, Y.; Bairagi, K.; Kelai, M.; Dappe, Y. J.; Lagoute, J.; Girard, Y.; Rousset, S.; Repain, V.; Barreteau, C.; Brandbyge, M.; Smogunov, A.; Bellec, A. Negative Differential Resistance in Spin Crossover Molecular Devices. **2022**. https://doi.org/10.48550/ARXIV.2206.13767.